SCIENCE CHINA
Information Sciences

• RESEARCH PAPER •

December 2016, Vol. 59 122304:1–122304:14
doi: 10.1007/s11432-015-5482-8

A novel RHT-TBD approach for weak targets in HPRF radar

Hongbo YU*, Guohong WANG, Wei WU & Shuncheng TAN

Institute of Information Fusion, Naval Aeronautical and Astronautical University, Yantai 264001*, China*

Received August 28, 2015; accepted October 11, 2015; published online April 22, 2016

Abstract A novel approach, which can handle ambiguous data from weak targets, is proposed within the randomized Hough transform track-before-detect (RHT-TBD) framework. The main idea is that, without the pre-detection and ambiguity resolution step at each time step, the ambiguous measurements are mapped by the multiple hypothesis ranging (MHR) procedure. In this way, all the information, based on the relativity in time and pulse repetition frequency (PRF) domains, can be gathered among different PRFs and integrated over time via a batch procedure. The final step is to perform the RHT with all the extended measurements, and the ambiguous data is unfolded while the detection decision is confirmed at the end of the processing chain. Unlike classic methods, the new approach resolves the problem of range ambiguity and detects the true track for targets. Finally, its application is illustrated to analyze and compare the performance between the proposed approach and the existing approach. Simulation results exhibit the effectiveness of this approach.

Keywords high pulse repetition frequency, weak targets, track-before-detect, randomized Hough transform, multiple hypothesis ranging, range ambiguity resolution

Citation Yu H B, Wang G H, Wu W, et al. A novel RHT-TBD approach for weak targets in HPRF radar. Sci China Inf Sci, 2016, 59(12): 122304, doi: 10.1007/s11432-015-5482-8

1 Introduction

In airborne radars, high pulse repetition frequency (HPRF) mode is widely used to provide an accurate velocity measurement against the clutter environment. However, with HPRF mode, radars may suffer from range ambiguity [1–3]. With the great development of stealthy technology, the newly available weak objects also bring new challenges to the target detection and tracking methods.

There are many classical techniques available for resolving range ambiguity, such as signal processing methods [4, 5], Remainder Theorem method (RT) [6, 7], Residues Difference Lookup Table method (RDT) [8] and hybrid filter method [9,10]. However, these methods have various drawbacks, as they rely on either the lower measurement error in the case of the signal method, or the higher signal-noise-ratio (SNR) in the case of the other methods. In [11, 12], the track before detect (TBD) approach is applied to process the data in HPRF radar, and a particle filter based TBD method (PF-TBD) is proposed to deal with ambiguous data for weak target. Although this is proved to perform well for weak targets with lower SNR, there exist two fundamental issues. Particle filter is so computationally expensive that

* Corresponding author (email: bluefishseasky@aliyun.com)

this approach is not practically achievable. The other drawback is that the spread measurements of high resolution may be required in order to suit the algorithm model, which, however, is unavailable for those commonly used medium/low resolution radar.

To address the above limitations, a randomized Hough transform based track before detect (RHT-TBD) approach is presented within the framework of multiple hypothesis mapping. In this method, the ambiguous measurements are adopted to offer spatial-temporal information for the implementation of TBD, which could be very valuable in helping tracking and detecting weak targets via HPRF radar. The major advantages of this novel RHT-TBD method are profoundly manifested in its better tracking performance and lower computational complexity compared to the PF-TBD method.

The content of this paper is organized in five sections as follows. Section 1 introduces the background and aim of this paper. In Section 2, the system dynamics model, system ranging model and system observation model are set up in a general scenario, and the tracking and detection problem in HPRF radar is described. The principle of our proposed method is presented in Section 3, along with its implementation. The simulation results are given in Section 4 and conclusion is finally summarized in Section 5.

2 System model and problem description

Before presenting our approach, let us review some basic concepts. For convenience, consider a general dynamic system as follows:

$$\begin{cases} \boldsymbol{X}_k = f(k, \boldsymbol{X}_{k-1}) + \boldsymbol{V}_{k-1}, \\ \boldsymbol{Z}_k = h(k, \boldsymbol{X}_k) + \boldsymbol{W}_k, \end{cases} \tag{1}$$

where $\boldsymbol{X}_k \in \mathbb{R}^n$ denotes the state of the target at time scan k with transition function f, $\boldsymbol{Z}_k \in \mathbb{R}^m$ denotes the measurement with observation function h. The state noise $\boldsymbol{V}_{k-1}$ and the measurement noise $\boldsymbol{W}_k$ are assumed to be independent and identically distributed processes.

2.1 System dynamics model

For the sake of simplicity, a single target moves with constant velocity in the X-Y plane is considered for a TBD scenario. At time scan k, the target state is defined as

$$\boldsymbol{X}_k = [x_k, \dot{x}_k, y_k, \dot{y}_k, \varepsilon_k]^{\mathrm{T}}, \tag{2}$$

where (x_k, y_k), $(\dot{x}_k, \dot{y}_k)$ and ε_k denote the position, velocity and the radar cross section (RCS) of the target, respectively. In general, it is assumed that the target RCS is not fluctuating. To model the moving dynamics of this target, we use the Newtonian equations of motion, whose discrete form can be written as follows:

$$\boldsymbol{X}_{k+1} = \boldsymbol{F}\boldsymbol{X}_k + \boldsymbol{G}\boldsymbol{v}_k, \tag{3}$$

where $\boldsymbol{F}$ is the state transition matrix, $\boldsymbol{G}$ is the process noise distribution matrix:

$$\boldsymbol{F} = \begin{bmatrix} 1 & T & 0 & 0 & 0 \\ 0 & 1 & 0 & 0 & 0 \\ 0 & 0 & 1 & T & 0 \\ 0 & 0 & 0 & 1 & 0 \\ 0 & 0 & 0 & 0 & 1 \end{bmatrix}, \tag{4}$$

$$\boldsymbol{G} = \begin{bmatrix} 0.5T^2 & 0 & 0 \\ T & 0 & 0 \\ 0 & 0.5T^2 & 0 \\ 0 & T & 0 \\ 0 & 0 & 1 \end{bmatrix}, \tag{5}$$

where T is the sensor sampling period, and $\boldsymbol{v}_k$ denotes the zero-mean white Gaussian process noise with zero mean and diagonal covariance matrix $\boldsymbol{Q}$:

$$\boldsymbol{Q} = \begin{bmatrix} \sigma_x^2 & 0 & 0 \\ 0 & \sigma_y^2 & 0 \\ 0 & 0 & \sigma_\varepsilon^2 \end{bmatrix}, \tag{6}$$

where σ_x^2 and σ_y^2 are the acceleration process noise variance in X and Y direction, respectively, and σ_ε^2 is the RCS variance.

2.2 System ranging model

Ranging is one of the basic functions for radar, which is realized based on the time delay between the transmission of a radar pulse and the reception of the corresponding echo. If the measured time delay from transmission to the received target echo pulse is t_R, the target range can be written as

$$R = \frac{1}{2} c t_R, \tag{7}$$

where c is the velocity of light. According to (7), the maximum accuracy range one can determine is $R_u = 0.5cT_r$, given the radar pulse repetition interval (PRI) T_r, where R_u is normally called the maximum unambiguous range (MUR).

In HPRF radar, the PRI is so low that the target echo of interest may arrive at the radar with delay greater than the PRI, leading to a possible ambiguous time delay:

$$t_{\text{amb}} \equiv t_{\text{true}} \bmod (T_r), \tag{8}$$

where t_{true} is the true delay time between the transmission pulse and the corresponding target echo and $\text{mod}(\cdot)$ implies modulo of the true delay time. In this situation, an ambiguous range $\tilde{r}$ may be derived from the function (7), giving a smaller range reading than the true range r_{true}:

$$\tilde{r} = \frac{1}{2} c t_{\text{amb}} = r_{\text{true}} \bmod (R_u). \tag{9}$$

2.3 System observation model

Let us assume that there is a two-coordinate radar located at the origin of the system coordinate, which observes a region in the X-Y plane. A useful mode of radar operation is used in our scenario, in which three PRFs switch in sequence among different scans. It is assumed that the set of PRFs is denoted by $F_{rf}, f = 1, 2, 3$. Suppose the fth PRF, F_{rf} among the above set, is selected, then the corresponding PRI and MUR can be written as

$$T_{rf} = \frac{1}{F_{rf}}, \tag{10}$$

$$R_{uf} = \frac{1}{2} c T_{rf}. \tag{11}$$

At each time scan k, the radar provides a set of measurements $\boldsymbol{Z}_k = \{\boldsymbol{z}_k^{(i,j)}\}$. The element $\boldsymbol{z}_k^{(i,j)}$ indicates the echo intensity value of the (i, j) pixel in the observation image, where $i = 1, 2, \ldots, N_x$ and $j = 1, 2, \ldots, N_y$ $j = 1, 2, \ldots, N_y$. Each pixel represents a region in the plane of size $\Delta_x \times \Delta_y$. Let $x_{\min}, y_{\min}$ represent the minimum detection range in the corresponding direction, thus the (i, j) pixel is centered in $[x_{\min} + (i - 0.5)\Delta x, y_{\min} + (j - 0.5)\Delta y]$.

If a point target $\boldsymbol{X}_k = [x_k, \dot{x}_k, y_k, \dot{y}_k, \varepsilon_k]^{\text{T}}$ is present in the observation region, the sensor will receive a target return echo and pass it to the signal processing component, producing a reading. However, in HPRF radar, the target will appear to be much near than the true position, when its distance exceeds

the MUR of radar. According to (8), the relationship between the measurement space and the target state can be established as follows.

Apparent target range:

$$\tilde{r}_k = \sqrt{x_k^2 + y_k^2} \bmod (R_{uf}) + w_r. \tag{12}$$

Target azimuth:

$$\alpha_k = \arctan\left(\frac{y_k}{x_k}\right) + w_\alpha, \tag{13}$$

where w_r and w_a are the measurement range error with variance σ_r^2 and the measurement azimuth error with variance σ_a^2, respectively, then by a coordinate transformation from polar coordinates to Cartesian coordinates, one can get the apparent target position (χ_k, γ_k):

$$\begin{cases} \chi_k = \tilde{r}_k \sin(\alpha_k), \\ \gamma_k = \tilde{r}_k \cos(\alpha_k), \end{cases} \tag{14}$$

and its corresponding pixel (I_k, J_k) in the echo image:

$$\begin{cases} I_k = \mathrm{Int}\left(\dfrac{\chi_k - x_{\min}}{\Delta x}\right), \\ J_k = \mathrm{Int}\left(\dfrac{\gamma_k - y_{\min}}{\Delta y}\right), \end{cases} \tag{15}$$

where the function $\mathrm{Int}(\cdot)$ means to take the closest integer of the variable. Therefore, the measurement of the (i, j) pixel can be written as

$$\boldsymbol{z}_k^{(i,j)} = \begin{cases} h_k^{(i,j)}(\boldsymbol{X}_k, \varepsilon_k) + \boldsymbol{w}_k^{(i,j)}, & \text{if } i = I_k \text{ and } j = J_k, \\ \boldsymbol{w}_k^{(i,j)}, & \text{else}, \end{cases} \tag{16}$$

where $h_k^{(i,j)}(\boldsymbol{X}_k, \varepsilon_k)$ denotes the reflection power at pixel (i, j) from the target $\boldsymbol{X}_k$, and $\boldsymbol{w}_k^{(i,j)}$ is the complex Gaussian noise sequences with variance σ_w^2. Hence, the signal to noise ratio (SNR) can be written as

$$\mathrm{SNR} = 10 \log \frac{h_k^{(i,j)}(\boldsymbol{X}_k, \varepsilon_k)}{\sigma_w^2}. \tag{17}$$

According to [13], $h_k^{(i,j)}(\boldsymbol{X}_k, \varepsilon_k)$ will be

$$h_k^{(i,j)}(\boldsymbol{X}_k, \varepsilon_k) = \frac{P_t G_t^2 \varepsilon_k \lambda^2}{(4\pi)^3 r_{\mathrm{true}}^4}, \tag{18}$$

where P_t is the radar transmitting power, G_t is the antenna gain, ε_k is the RCS of target and λ is the wavelength of the radar signal.

2.4 Problem analysis

Based on the above assumption, the tracking problem can be formulated as determining the trajectories according to the measurements set. However, the classical tracking methods cannot perform efficiently here, because the measuring position of targets, in HPRF radar, will be different from its true position. Additionally, the difficulty will increase significantly in the case of weak targets, for the false alarm or miss detection caused by low SNR. For high SNR, the problem can be decomposed into a three-stage process, the detection step, the ambiguity resolution step and the track forming step. In the first step, a detection threshold is used to eliminate undesired interference (like clutter or jamming), where the output are the ambiguous measurements. The next step is to resolve the measurement ambiguity with some classical method, such as the RT and the RDT. Finally, tracks are made from these unambiguous measurements by means of data association and filtering. Unfortunately, the above approach does not

comply in the case of lower SNR, where the decision of the detection threshold fails to find an acceptable compromise between false alarm and miss detection.

For low SNR targets, an alternative approach, referred to as TBD, is usually used to improve detection performance and tracking accuracy. Different to the classical approaches which may result in information loss, TBD makes the detection decision using the track results over time, in which the information is integrated over multiple scans [14,15]. This is acceptable in general low PRF system. However, in HPRF radar, which provides ambiguous measurements, there will be some difficulty in implementation of TBD. The reason is that the ambiguous measurements may destroy the continuity of target plots along the trajectory, which is essential for accumulating information in the frame of TBD.

Therefore, tracking weak targets with ambiguous measurements will be of great difficulty since the trajectory is folded in the measurement space, and the classical tracking strategy must be redesigned to suit the weak target in HPRF radar.

3 Proposed algorithm introduction

In this section, a RHT-TBD approach within the framework of multiple hypothesis mapping will be used to solve our problem. In this method, a multiple hypothesis ranging process (MHR) is firstly used to extract the spatial-temporal information from the ambiguous measurements. Then the RHT approach is applied into the framework of TBD, which tracks and detects weak targets via HPRF radar. Further details are given in the next section.

3.1 Multiple hypothesis ranging

For convenience, consider a target trajectory wholly in the first quadrant of the radar observation region. Given the minimum detectable signal of the radar, $S_{\min}$, the maximum detection rang R_m can be written as [13]

$$R_m = \left[\frac{P_t G_t^2 \varepsilon_k \lambda^2}{(4\pi)^3 S_{\min}}\right]^{1/4}. \tag{19}$$

Thus, according to the assumption in Section 2, the ranging region of radar can be divided into several range ambiguity intervals (RAI), S_f^l, $l \in [0, \ldots, L_f]$ (see Figure 1). And S_f^l represents a torus between two circles, of which the radiuses are $(l-1)\cdot R_{uf}$ and $l \cdot R_{uf}$, respectively. The set of integers $[0, \ldots, L_f]$ is referred to as the pulse interval numbers (PIN), with L_f determined by the maximum detection rang R_m:

$$L_f = \mathrm{Int}(R_m / R_{uf}). \tag{20}$$

Let the sequence of A, B, C and D, marked with red asterisks, be the true target position, which is apparently continuous in the real-world space. However, in the measurement space, the apparent trajectory becomes the discontinuous sequence of a, b, c and d, due to the range folded effect in HPRF radar [11]. Thus, the traditional TBD method must be modified to deal with those discontinuous measurements. To extract the spatial-temporal information from the discontinuous measurements, the multiple hypothesis idea [16] is incorporated into our method, which is called the multiple hypothesis ranging (MHR) procedure. Consider the apparent plot a for example, of which the apparent range, azimuth and echo intensity are $\tilde{r}_k^f$, α_k and φ_k, respectively. Since, in practical application, the true position of plot a is unknown, it may come from every RAI. In our method, a vector of possible ranges can be created by mapping the apparent position into each of the RAI area as follows:

$$\bar{r}_k^f(l_f) = (l_f - 1) \times R_{uf} + \tilde{r}_k^f, l_f = 1, \ldots, L_f. \tag{21}$$

Considering the unambiguous azimuth α_k, the possible positions $[\bar{x}_k^f(l_f), \bar{y}_k^f(l_f)]$ of plot a, can be written as follows:

$$\begin{cases} \bar{x}_k^f(l_f) = \bar{r}_k^f(l_f) \cdot \cos\alpha_k, \\ \bar{y}_k^f(l_f) = \bar{r}_k^f(l_f) \cdot \sin\alpha_k, \end{cases} \quad l_f = 1, \ldots, L_f. \tag{22}$$

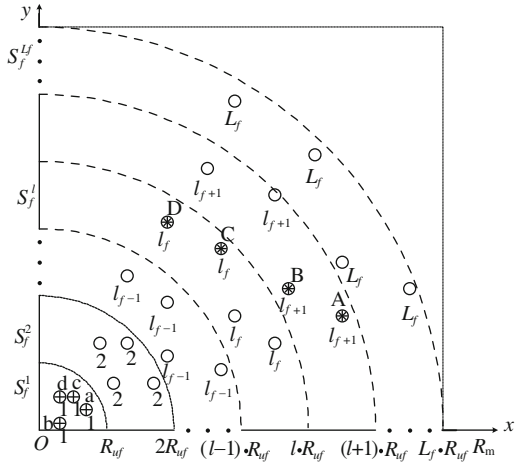

Figure 1 Illustration of MHR mapping.

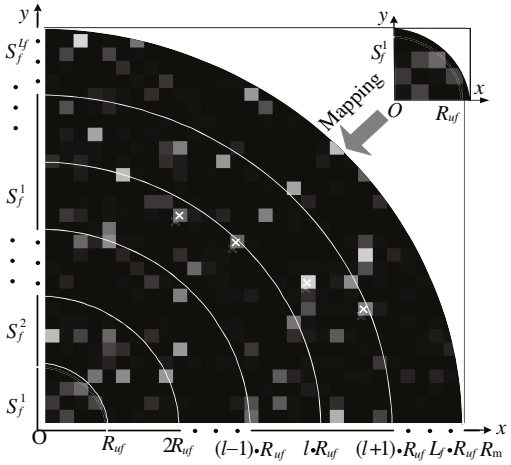

Figure 2 Measurements after MHR processing.

Similarly, all of the four plots a, b, c and d can be mapped into the MHR space as marked by hollowed circles in Figure 1. The number at the bottom of each circle denotes the PIN to the corresponding possible position of each plot.

From Figure 1, one can see that there surely exist such a set of PINs enabling the possible positions of a, b, c and d to coincide with the true positions A, B, C and D in the coordinate. From this point of view, the problem of ambiguity resolving can be reduced to the simple tracking problem, i.e. extraction of the target position from the possible positions.

3.2 Randomized Hough transform based TBD

Considering the low SNR of weak targets, where clutter or noise may cause strong interference, the measurement environment must be far more complex than that in Figure 1. According to the system observation model in Subsection 2.3, measurements of the target with low SNR (3 dB, for example) exceeding a primary threshold can be mapped by the MHR method into the possible RAI spaces as shown in Figure 2.

In Figure 2, the brightness of each pixel location corresponds to the intensity resulting at that location, originating from either targets or undesired interference. The panel on the top right is the original ambiguous measurements within a scanned sector of radius R_{uf}. After MHR processing, the original data are mapped into all the possible RAI space, illustrated by the bottom-left panel in the figure, where the cross indicates target true position. In this way, the discontinuous measurements of our interest become linear in the MHR space, making possible the echo intensity integration over time by TBD. Hence, the complex problem of HPRF radar weak targets detection and tracking can be simplified to the general TBD problem.

To extract the desired target position, the randomized Hough transform (RHT) is applied to accumulating the target information in each bin of the MHR measurements. Before presenting the RHT method, let us review the standard Hough transform (HT), in which the difficulty of global detection in data space can be reduced to the much simpler peak detection in parameter space [17]. As illustrated in Figure 3, each measurement point (x, y) in the Cartesian coordinates can be mapped to a sine curve via

$$\rho = x\cos\theta + y\sin\theta, \quad \theta \in [0, \pi]. \tag{23}$$

By discretizing the HT parameter space with resolution $\Delta\rho$ and $\Delta\theta$, a set of accumulators is generated with each cell corresponding to a belt in the measurement space. From Figure 3, we can see that for a set of points $(x_i, y_i)\,, i = 1, 2, 3$ lying in a straight-line, there is surely a pair of parameters (ρ_0, θ_0), satisfying

$$y_i = \frac{\rho_0}{\sin\theta_0} - \frac{1}{\tan\theta_0}x_i, \tag{24}$$

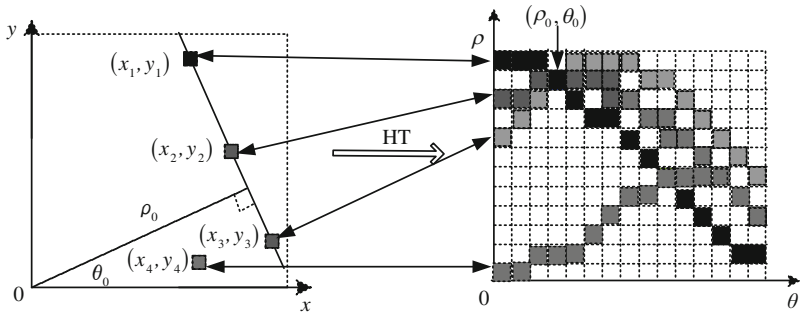

Figure 3 Sketch map of Hough transform.

and the points without this straight-line cannot be mapped into (ρ_0, θ_0), such as the point (x_4, y_4). In other words, a set of points can be accumulated in a parameter cell by HT, if and only if they belong to the same straight-line. Hence, if one detects the peak cell in HT space, the corresponding straight-line can be estimated by inverse HT transformation. Unfortunately, the implementation of HT is rather computationally involved, which prevents it from practical application in our approach. For processing the great number of measurements in MHR space, the RHT is used to reduce the computational complexity [18, 19]. The RHT is an improved algorithm for the standard HT. Unlike the standard HT, which can be viewed as a one-to-many mapping, RHT defines a many-to-one mapping from a set of measurement points to some parameter cell. In the RHT, points in the Cartesian coordinates are mapped to the most possible parameter cell rather than all the possible cells as in the standard HT, which will greatly reduce the computational requirements. Let $D = \{d_i\}$, $i = 1, 2, \ldots, I$ be the set of all points in MHR space, where $d_i = \{(x_i, y_i, \varphi_i)\}$ denotes the center of the resolution cell in X and Y direction, and the corresponding echo intensity, respectively. We randomly choose two points d_i and d_j out of the set and a parameter pair (ρ_u, θ_v) can be written by solving the following equation:

$$\begin{cases} \rho_u = x_i \cos\theta_v + y_i \sin\theta_v, \\ \rho_u = x_j \cos\theta_v + y_j \sin\theta_v. \end{cases} \tag{25}$$

Such that, the two point's intensity can be accumulated in the parameter cell (ρ_u, θ_v):

$$(\varphi_m + \varphi_n) \to H(u, v), \tag{26}$$

where $H(u, v)$ indicates the intensity accumulator array with respect to the parameter cell (ρ_u, θ_v). Assuming that the undesired interference is distributed randomly across the observation region, MHR measurements originating from the same target will be mapped into the same parameter space accumulator, while measurements from the strong interference will be mapped randomly across the parameter space. After a certain number of sampling, one can get the histograms of accumulation intensity, in which the accumulator cell defining the target trajectory will contain more intensity than others. Consequently, the unambiguous track can be detected by searching peaks in the parameter space. Finally, the corresponding PIN of original measurement can be achieved by reverse mapping from the detected trajectory to the MHR space.

3.3 Implementation of the algorithm

By combining the RHT method with a MHR procedure, we obtain the proposed RHT-TBD approach for tracking and detecting weak targets in HPRF radar, which consists of 7 steps, see Figure 4. Given the system model as described in Section 2, the proposed algorithm proceeds as follows:

Step 1. Primary threshold

At each time scan, a lower primary threshold is set in the measurement space, against which the raw data is compared. The output of this function is the ambiguous measurements. Since the main objective of this step is to reduce the computation load, the primary threshold must allow most of the

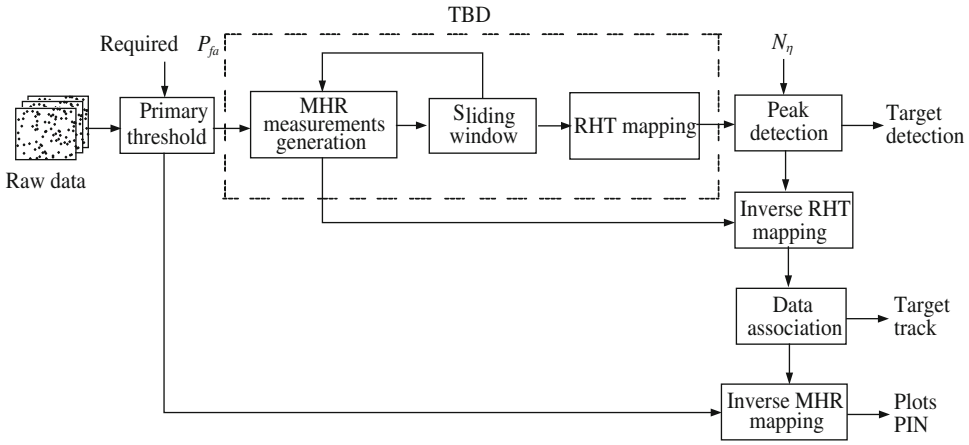

Figure 4 System block diagram.

radar returns. In this way, all of the target information can be preserved while much of the clutter is eliminated. Generally, the primary threshold is given in the form of the desired value of the primary probability of false alarm [14]:

$$\eta_1 = -\ln(P_{fa}), \tag{27}$$

where P_{fa} denotes the desired probability of false alarm.

Step 2. MHR processing

In this step, measurement pixels exceeding the primary threshold are mapped into all the possible RAI spaces by the MHR procedure, generating the MHR readings. Since the RHT method uses data over a batch of measurements, we apply sliding window storage (length m) to improve the real-time property of the algorithm. Each entry in the window represents a complete MHR scan necessary for performing the RHT-TBD processing. When a new scan is inserted into the window, the oldest scan is shifted out. Hence, the column size of the sliding window is kept constant to m scans.

Step 3. RHT mapping

We are now ready for performing the RHT in the framework of TBD, and this step is comprised of three procedures.

First, initialize the parameter space, and let all the bins in the accumulation array $H(u, v)$ be zero;

Second, let D denote the set of all the MHR measurements from MHR window. Randomly pick n-point pairs (d_i, d_j) from D, and solve the parameter point (u, v) using the curve equation (28) with (d_i, d_j);

Third, accumulate the corresponding accumulator cell $H(u, v)$ in parameter space and continue with the second procedure.

Step 4. Peak detection

The RHT mapping step must run long enough to get a global peak detection in the parameter space. Then each accumulator cell is normalized to unit power before comparing to a preset threshold N_η. The cell reaching N_η describes the parameter of a detected target, as a peak $H(u_p, v_p)$.

Step 5. Track estimate

By the inverse RHT mapping, those higher peaks are transformed to a set of potential target pots in the MHR image. However, these pots are not the actual target track, since there are some false measurements. Therefore, a data association procedure is needed to make best use of the sequence order and the prior knowledge, which finally establishes the correct track estimate.

Step 6. Ambiguity resolving

Finally, the corresponding PIN of each PRF can be achieved by the reverse mapping from the detected trajectory to the raw data. Thus, we succeeded in solving the range ambiguity problem.

Table 1 Parameter set

Parameter	Value
Radar sampling period (s)	$T = 2$
Total simulation scans	$K = 25$
Radar transmit power (km)	$P_t = 10$
Radar Wavelength (m)	$\lambda = 0.1$
Radar antenna gain	$G = 10^4$
Radar maximum detection range (km)	$R_m = 150$
Range measurement error standard deviation (m)	$\sigma_r = 100$
Azimuth measurement standard deviation	$\sigma_b = 0.5^\circ$
Pulse repetition frequency (PRF) (kHz)	$F_{r1} = 119, \quad F_{r2} = 114, \quad F_{r3} = 194$
Target RCS (m^2)	$\sigma = 10$

4 Simulations and discussion

In order to test the performance of this novel method, a generalized scenario is applied in this section.

4.1 Simulation scenario

A two-dimensional coordinate example is presented in our simulation. It is assumed that a target moves towards the sensor with a constant velocity of (0.12 km/s, 0.33 km/s), and the initial position is at (27 km, 38 km) in the X-Y plane. Data is simulated according to the models given in Section 2, and the measurement plots comprise range, azimuth and echo intensity. The target azimuth is measured relative to the true north at the radar location and the radar is at the origin of the coordinate system. Other parameters used in this simulation are listed in Table 1.

Substituting the above PRF value into (10) and (11) yields the corresponding PRI and MUR, T_{r1} = 8.4 μs, T_{r2} = 8.8 μs, T_{r3} = 5.2 μs, and R_{u1} = 1.26 km, R_{u2} = 1.31 km, R_{u3} = 0.77 km. Based on the above scenario, the proposed RHT-TBD method and the PF-TBD method from [11] are separately used to track and detect weak targets in HPRF radar. The simulation lasts 25 time steps and 100 runs of Monte Carlo simulation are performed to compare the performance between the two methods. To test the detection performance, simulations are made with respect to different SNR conditions (9 dB, 6 dB, 3 dB).

The simulated scenarios are given in Figure 5(a)–(c), where the peaks indicate the target echo in the presence of Rayleigh noises with different SNRs. In Figure 5(a), the SNR is higher and it is easy to discern the target plots with high peaks, while in Figure 5(c) with lower SNR, it is not possible to distinguish the target from the noise. And in Figure 5(b), where the SNR is a compromise between Figure 5(a) and (c), only a part of target plots can be extracted from the image. Since the sensor is located at the origin of the system coordinate in our scenarios, the distance between the sensor and target exceeds the MUR of three PRFs, which will result in ambiguous measurements. Figure 5(d)–(f) illustrate the corresponding measurements with three SNRs, where the brightness of each pixel location indicates to the intensity at that location, originating from either targets (marked with white circle) or undesired interference. Figure 5 shows that the target plots, in the case of HPRF, become discontinuous in comparison with the real trajectory as in the simulated scenario. Furthermore, the lower SNR will increase the difficulty of target detection.

4.2 Effectiveness analysis

Generally, the TBD algorithm is used to track and detect weak targets with lower SNR. The traditional TBD, however, is unsatisfactory in this situation, since the discontinuous measurements prevent the target information from accumulating over time and position. Owing to the MHR procedure, the proposed approach can convert the discontinuous measurements into the normal state, which can be used in the framework of TBD.

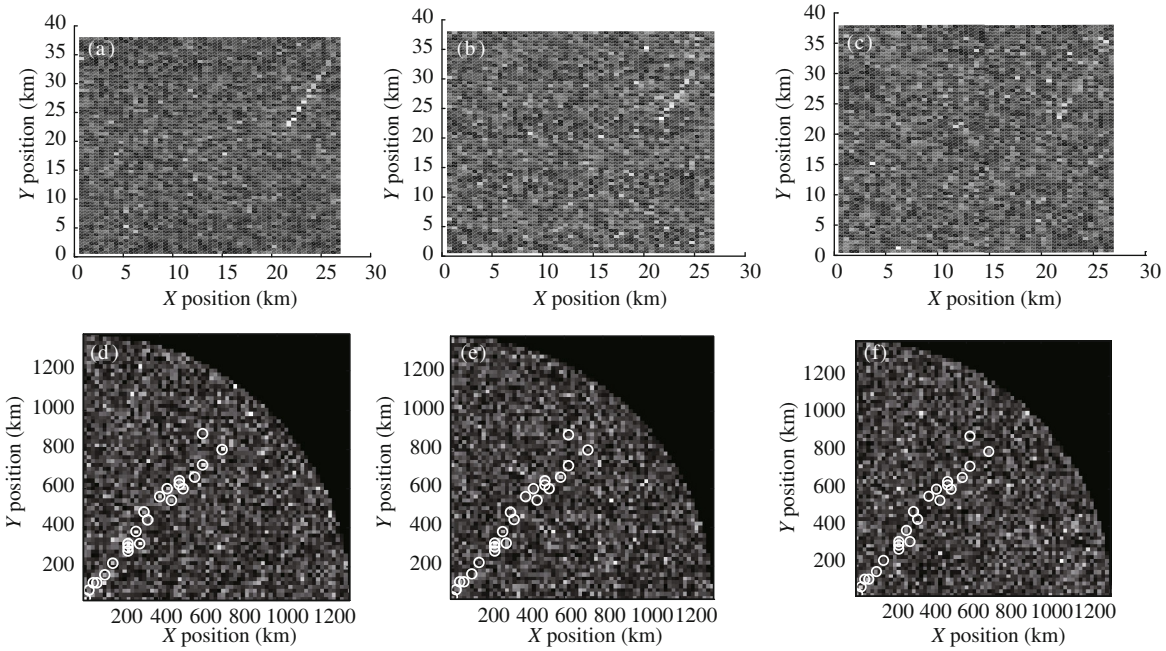

Figure 5 The simulated scenarios and the associated ambiguous measurements with different SNRs. Simulated scenario with (a) SNR = 9 dB; (b) SNR = 6 dB; (c) SNR = 3 dB; and measurements with (d) SNR = 9 dB; (e) SNR = 6 dB; (f) SNR = 3 dB.

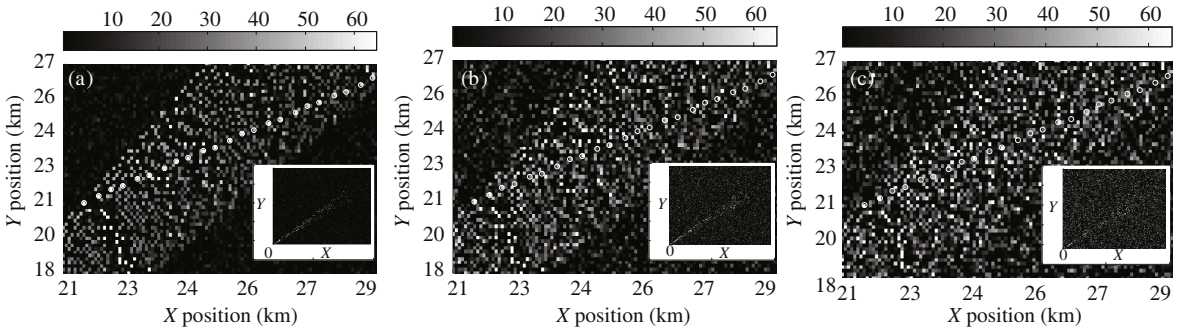

Figure 6 The MHR measurements with different SNRs. (a) SNR = 9 dB; (b) SNR = 6 dB; (c) SNR = 3 dB.

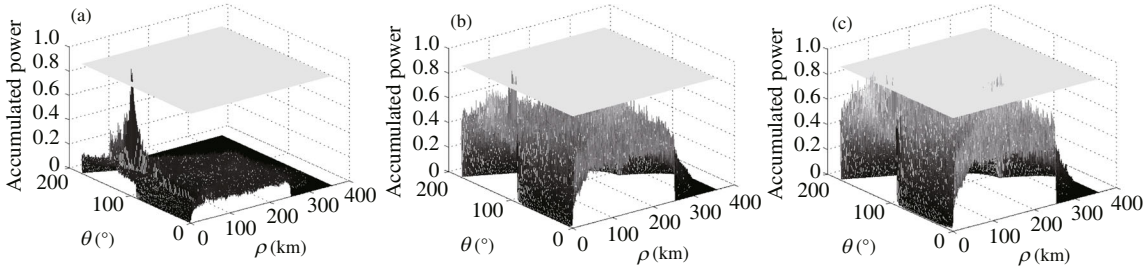

Figure 7 RHT parameter space mesh plot. (a) SNR = 9 dB; (b) SNR = 6 dB; (c) SNR = 3 dB.

Figure 6 shows the processed measurement results after the MHR procedure, where the major data in each of the three diagrams is a zoom-in version of the associated lower-right boxed region. From Figure 6, we can see that the measurement outputs from HPRF radar, which are discontinuous and ambiguous (see Figure 5(d)–(e)), have been restructured to provide a location near its real position (marketed with white circle). With the MHR procedure, the weak target can be tracked and detected. Next, the RHT approach is applied into the framework of TBD.

Figure 7 shows the RHT parameter space based accumulated power with different SNRs, corresponding

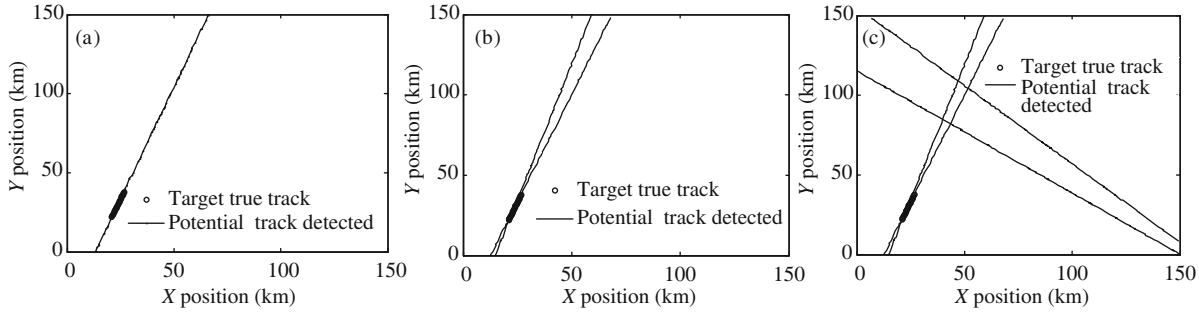

Figure 8 Potential target tracks detected with threshold $N_\eta = 0.9$. (a) SNR = 9 dB; (b) SNR = 6 dB; (c) SNR = 3 dB.

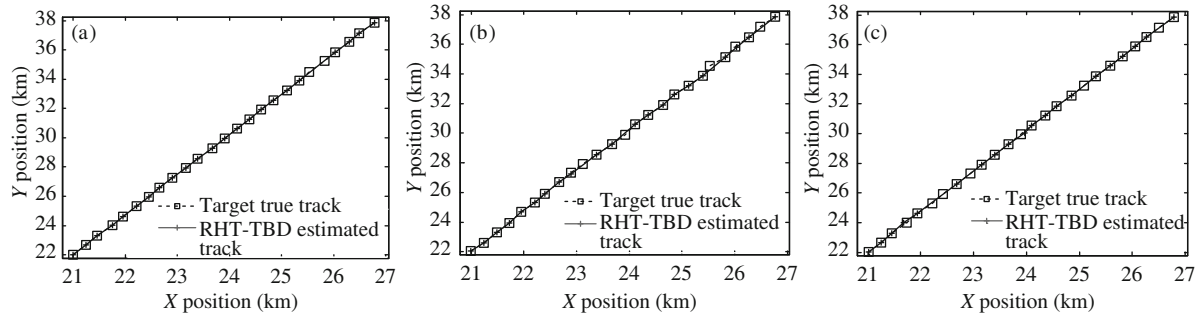

Figure 9 RHT-TBD estimated target track with different SNRs. (a) SNR = 9 dB; (b) SNR = 6 dB; (c) SNR = 3 dB.

to the MHR measurements in Figure 6. Note that, the accumulated array here has been normalized to unity. To declare target detections, the parameter cells must be compared against a preset threshold N_η. The choice of N_η is a significant issue to the implementation of the TBD, since a higher threshold may filter out the actual target track while a lower threshold lead to a great number of potential target paths. In this paper, $N_\eta = 0.9$ is used as an acceptable compromise between these contradictory requirements, which is denoted by a gray surface in each mesh plot. Higher peaks that exceed the threshold are declared as potential targets, which correspond to a set of plots in the MHR image. By an inverse RHT process, those higher peaks are mapped to a set of potential target tracks, see Figure 8. From Figures 7 and 8, we can see that, with a higher SNR, only one peak cell exceeds the detection threshold, which produces a potential target tracks with few false plots, while a lower SNR results in many potential target tracks and thus leading to a large number of false plots.

Now, we get a set of possible tracks after a threshold process, by which almost all the undesired interferences are eliminated. However, the actual target track is not achieved, since there are some false plots in the potential target tracks. This may be realized by a data association approach in relation to the sequence order of measurements and the prior knowledge of targets. Finally, we arrive at the estimated track as shown in Figure 9.

Next, let us consider the detection performance of the proposed method. The RHT-TBD is implemented in the data domain of radar measurements, where the main idea is to realize the non-coherent integration of target intensity along the potential trajectory. Based on the correlation of the signal's amplitude regardless of the phase information [20], the application of RHT-TBD must meet the foundational premise where the mean amplitude of the target is higher than that of the noise. Therefore, the lower limit of SNR for the RHT-TBD method is 0 dB in theory. For lower SNR below 0 dB, the target peaks might be submerged by the powerful noise peaks, which will invalidate the non-coherent integration of RHT-TBD. To further improve the SNR of weak target, the focus before detect (FBD) approach is proposed in [20–22], in which both the amplitude and phase information can be used to realize the coherent integration of target intensity. With the Doppler compensation function, the FBD provides a new way to further improve the SNR for weak target detection, and it can be applied in case where the simple integration of TBD would be inefficient because of the lower SNR. In future work, we

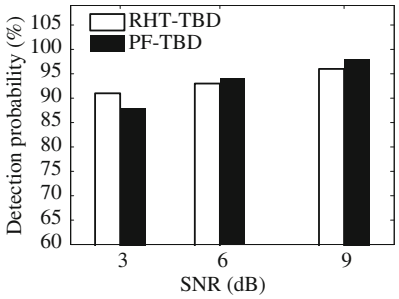

Figure 10 Comparison in detection performance between two approaches with different SNRs.

would consider the combination of FBD and the proposed method in this paper, and gain insights about this problem.

4.3 Performance comparisons

To further illustrate the performance of our proposed RHT-TBD approach, a comparison to the PF-TBD approach in [11] is given based on the above scenario, under the condition that the number of particles is set to $N_{\mathrm{PF}} = 3000$ and the target survival probability is $p_{\mathrm{exist}} = 0.95$ as in [11]. The results for the experiments are depicted in Figures 10 and 11, and they were obtained by averaging over 100 runs of simulations.

Figure 10 shows the average probability of correct detection for different SNRs with the primary probability of false alarm as $P_{fa} = 10^{-3}$. It can be seen that the detection probability of both methods decreases with the decreasing SNRs. The proposed approach, of which the detection probability exceeds 90% with three SNRs, is much less sensitive to SNR than the PF-TBD algorithm. For the high SNR, the RHT-TBD method provides a much lower performance in detection than that of the PF-TBD approach, while for the low SNR, it is vice versa. The reason is that, with lower SNR, the relatively high noise may produce a much more uniform distribution of the particle weights in PF-TBD, which leads to an inaccurate particle model in the resampling stage, and thus resulting in a lower detection performance. However, as a patch process, the RHT-TBD may reduce the high noise effect of lower SNR, since the position cell of the noise spikes are uncorrelated from scan to scan. If only the mean amplitude of the target is higher than that of the noise, the target peaks resulting from the non-coherent integration along the target true trajectory would exceed that along the false trajectory. Therefore, the detection of RHT-TBD outperforms that of PF-TBD in lower SNR.

Figure 11 compares the tracking results of two methods in the form of tracking position root mean square errors (RMSE). Simulation result shows that, based on the correct detection, both of the two approaches may accurately estimate the target track. During the first several steps, the track estimation of is a bit indecisive with fluctuating RMSE, however it converges to the true trajectory after some scans. With the SNR increasing, the RMSE for both methods gradually reduces, thereby the smaller the RMSE, the more accurate the track estimate. It can also be seen that the tracking accuracy of the proposed method is superior to that of the PF-TBD.

Finally, let us consider the computational complexity of the above two methods. Being an iterative method comprising of seven steps, the PF-TBD approach is computationally extensive, which is its main drawback. At each iteration, the computational complexity of this multiple-step processing algorithm can be expressed as the sum complexity of all steps. The PF-TBD approach has 4 major computational units: sampling period, particle prediction, weight computation, and state estimate, of which the particle prediction step and the weight computation step take the most calculations among the whole process. If n is the number of particles, then the time complexity of the particle prediction step is $O(n^2)$ [23]. In order to accumulate all the information of the weak target, the measurement in the PF-TBD algorithm is extended to the form of point spread function. Thus, the weight computation operation is of complexity $O(nm^{m_x})$, where m, m_x denote the number of measurement pixels and the dimension of the measurement

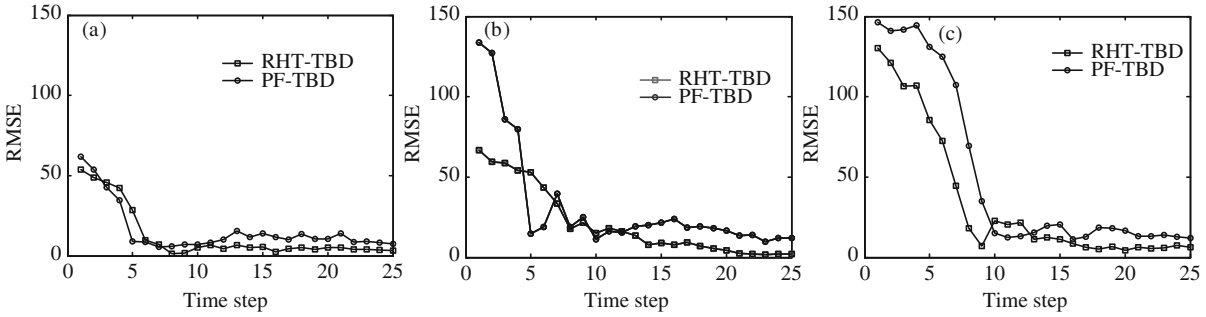

Figure 11 Comparison in tracking performance between two approaches with different SNRs. (a) SNR = 9 dB; (b) SNR = 6 dB; (c) SNR = 3 dB.

Table 2 Average time used for two methods with different SNRs

SNR	3 dB	6 dB	9 dB
PF-TBD	2.177 s	2.175 s	2.125 s
RHT-TBD	1.386 s	1.162 s	0.800 s

vector respectively. The whole procedure of PF-TBD has time complexity at least $O(n^2) + O(nm^{m_x})$, where $m_x = 3$ according to [11]. As a batch procedure, the proposed RHT-TBD method is much less complex. According to [24], its computational complexity is of the order much lower than $O(r_t m^{p_x})$, where r_t is a small number, and p_x represents the dimension of the parameter space, in this paper $p_x = 2$. Overall, the proposed RHT-TBD approach has a great advantage in the computational complexity over the PF-TBD approach. To validate this, experiments on the same scenario with different SNRs have been carried out. The time reported is for a standard computer running Matlab 7.0 under the Windows XP operating system. The platform is a microcomputer consisting of four Intel(R) Core(TM) Quad CPUs (2.33 GHz). Table 2 shows the average time from 100 trials of simulations, from which, we can reach the following conclusion:

1. The proposed RHT-TBD approach has a great advantage in the computational complexity over the PF-TBD approach;

2. The lower the SNR, the longer would be the processing time. Since the low SNR will result in more false measurements exceeding the primary threshold, the average running time, for both of the two methods, grows linearly with the decreasing SNR;

3. With increasing SNR, the average time for PF-TBD drops slowly while that for RHT-TBD drops much more quickly. The reason is that the computational complexity of RHT-TBD depends largely on the amount of current measurements. However, the main factor which affects the computational complexity of PF-TBD is the number of sampling particles.

5 Conclusion

A novel RHT-TBD based approach, which can handle ambiguous data of weak targets, is proposed and evaluated in this paper. To make best use of the relative information hidden in the ambiguous measurements, a multiple hypothesis ranging procedure is incorporated into the TBD framework for the first time, which is capable of integrating the data energy along potential target trajectory. The ambiguous data is revaluated while the track detection is made at the end of the processing chain, which directly estimates the target position, avoiding the loss tracking of the weak target. Different to classic methods, the proposed approach transforms the problem of range ambiguity resolution into the decision of the real track for targets, which provides a new outlook to such problem. Finally, illustrative simulations are given to compare the performance between the proposed approach and the PF-TBD, with respect to different SNR. The results demonstrate that the proposed algorithm provides great advantage in the detection and tracking of the weak targets in HPRF radar. Besides, its computational complexity is

much less than that of the PF-TBD method.

Acknowledgements This work was supported by National Natural Science Foundation of China (Grant Nos. 61179018, 61372027, 61501489) and Special Foundation for Mountain Tai Scholars.

Conflict of interest The authors declare that they have no conflict of interest.

References

1 Wang G H, Tan S C, Guan C B. Multiple model particle filter track-before-detect for range ambiguous radar. Chinese J Aeronaut, 2013, 6: 1477–1487
2 Wang W Q. Mitigating range ambiguities in high-PRF SAR with OFDM waveform diversity. IEEE Geosci Remote Sensing Lett, 2013, 1: 101–105
3 Raney R K, Freeman A, Jordan R L. Improved range ambiguity performance in Quad-pol SAR. IEEE Trans Geosci Remote Sensing, 2012, 2: 349–356
4 Xie W, Zhang B, Wang Y, et al. Range ambiguity clutter suppression for bistatic STAP radar. EURASIP J Advances Signal Process, 2013, 1: 1–13
5 Thomas A G, Berg M C. Medium PRF set selection: an approach through combinatorics. IEE Proc Radar Sonar Nav, 1994, 141: 307–311
6 Wang C, Yin Q Y, Wang W J. An efficient ranging method based on Chinese remainder theorem for RIPS measurement. Sci China Inf Sci, 2010, 53: 1233–1241
7 Lei W, Long T, Han Y Q. Resolution of range and velocity ambiguity for a medium pulse Doppler radar. In: the Record of the IEEE International Radar Conference, Alexandria, 2000. 560–564
8 Zhou R, Gao M G, Han Q Y. Resolving ambiguity for multiple targets using residues' difference lookup table (in Chinese). J Beijing Institute Tech, 2002, 4: 221–224
9 Wang N, Wang G H, Zeng J Y, et al. Range ambiguity resolving of HPRF radar based on hybrid filter. Sci China Inf Sci, 2011, 54: 1534–1546
10 Wang N, Wang G H, Guan C B, et al. A Bayes approach to simultaneous range ambiguity resolving and tracking for high pulse-repetition frequency radar. J Astronautics, 2011, 32: 2015–2022
11 Tan S C, Wang G H, Wang N, et al. Joint range ambiguity resolving and multiple maneuvering targets tracking in clutter via MMPHDF-DA. Sci China Inf Sci, 2014, 57: 082311
12 Bocquel M, Driessen H, Bagchi A. Multitarget particle filter addressing ambiguous radar data in TBD. In: the Record of the IEEE International Radar Conference, New York, 2012. 0575–0580
13 Richards M A, Scheer J A, Holm W A, et al. Principles of Modern Radar. Edison: SciTech Publishing, 2010. 64–66
14 Zhang P, Zhang L. An efficient track-before-detect algorithm based on complex likelihood ratio in radar systems. Sensors Transducers, 2014, 7: 299–305
15 Grossi E, Lops M, Venturino L. A heuristic algorithm for track-before-detect with thresholded observations in radar systems. IEEE Signal Process Lett, 2013, 8: 811–814
16 Wang H, Sun J P, Lu S T, et al. Factor graph aided multiple hypothesis tracking. Sci China Inf Sci, 2013, 56: 109301
17 Wu Z, Zhang J, Zhang L, et al. A novel Hough track initialization algorithm for multi-sensor environment. Sensor Lett, 2013, 4: 686–691
18 Fan L, Zhang X, Wei L. TBD algorithm based on improved randomized Hough transform for dim target detection. Progress Electromagnet Res, 2012, 31: 271–285
19 Zhang Y H, Su X H, Ma P J. Track initiation based on extended trellis and randomized Hough transform. Appl Mech Mater, 2012, 128: 1281–1287
20 Xu J, Yu J, Peng Y N, et al. Radon-Fourier transform for radar target detection (I): generalized Doppler filter bank. IEEE Trans Aerosp Electron Syst, 2011, 47: 1186–1202
21 Xu J, Yu J, Peng Y N, et al. Radon-Fourier transform for radar target detection (II): blind speed sidelobe suppression. IEEE Trans Aerosp Electron Syst, 2011, 47: 2473–2489
22 Xu J, Xia X G, Peng S B, et al. Radar maneuvering target motion estimation based on generalized Radon-Fourier transform. IEEE Trans Signal Process, 2012, 60: 6190–6201
23 Guo D, Wang X D. Quasi-Monte Carlo filtering in nonlinear dynamic systems. IEEE Trans Signal Process, 2006, 54: 2087–2098
24 Xu L, Oja E. Randomized Hough transform (RHT): basic mechanisms, algorithms, and computational complexities. CVGIP: Image Understanding, 1993, 57: 131–154